The Nu Class of Low-Degree-Truncated, Rational, Generalized Functions. II.

IMSPE in Design of Computer Experiments:

Low-N, Multifactor, Free-Ranging, Optimal Designs

Selden Crary[1], Richard Diehl Martinez[2],

Michael Saunders[2], Amin Mobasher[3], and Nikoloz Chkonia[4]

1. Palo Alto, CA, USA

2. Department of Management Science and Engineering
Stanford University, Stanford, CA, USA

3. San Jose, CA, USA

4. Computer Science Department
Hamilton College, Clinton, NY, USA

Abstract

In this Part II of a five-Roman-numeralled-part series, we report computed examples of $IMSPE$-optimal designs, as well as one near-optimal design, in the mathematical field of statistical design of computer experiments, all under Gaussian-correlation functions, except as specifically noted. In particular, we demonstrate the following eight types of phase diagrams and designs: (1) the two-factor, $n = 1$ phase diagram of optimal designs, over all hyperparameters, under the exponential-, Gaussian-, or either of two Matérn-correlation functions; (2) the similarly detailed, two-factor, $n = 2$ and $n = 3$ phase diagrams of optimal designs, over all hyperparameters, showing bird's-beak and sorcerer's-hat sub-domains; (3) a three-factor, triplet-point optimal design, with points on an equilateral triangle and interpoint separation of less than 10^{-33} over the $[-1,1]^3$ design domain; (4) a four-factor, quadruplet-point optimal design; (5) a five-factor, quintuplet-point optimal design; (6) a six-factor, sextuplet-point optimal design; (7) a two-factor, duet–twin-point optimal design; and (8) a two-factor, quartet–twin-point, near-optimal design.

Key Words: Gaussian process, Matérn process, covariance matrix, twin points, clustered design, asphericality.

1.   Introduction

In this Part II of the five-part series, we report computed examples of $IMSPE$-optimal designs in the mathematical field of statistical design of computer experiments, for designs with two through six factors, under Gaussian correlation functions, and with the integration taken over closed, (hyper-)cuboidal regions. Our $IMSPE$-optimal-design notation traces back to [1] and was written out verbosely in [2,3]. Section 3 contains detailed phase diagrams for two-factor, N-point designs for $n = 1, 2,$ and 3. Detailed two-factor phase diagrams for $N = 4$ and 11 were reported previously, see [2] and [4], respectively. Section 4 mentions a four-factor design with a pair of

twin points. Section 5 reports our discovery of d-uplet-point putatively optimal designs for $3 \leq d \leq 6$. Section 6 reports our discovery of a putatively optimal design with two twins – what we call a "duet–twin-point design." Section 7 summarizes these results. Finally, Section 8 reiterates our group's commitment to ICERM's recommendations on research reproducibility. These simple examples provide background for the development, in Parts III and IV of this series of papers, of a new class of special, generalized functions, which we have dubbed the "Nu-class of low-degree-truncated rational generalized functions," and for showing that the $IMSPE$ objective function is a member of this class.

2.   Outline

3.   Two-factor, $IMSPE$ -optimal-design phase diagrams

3.1 $n = 1$

We start with the trivial, two-factor, single-design-point case. Irrespective of the correlation-function parameter, for each case the $IMSPE$-optimal design was reported in [3] as a single point at the origin of the coincident, bi-unit-square, design and prediction regions. For reference, Table 1, below, summarizes formulas for the normalized $IMSPE$, along with the specific equation number in [3], for each of the following four correlation-function parameters: $\tilde{p} = 1$ for exponential correlation, $\nu = 3/2$ for the Matérn-3/2 correlation, $\nu = 5/2$ for the Matérn-5/2 correlation, and $\tilde{p} = 2$ for Gaussian correlation.

Correlation-function parameter	Eq.	IMSPE formula	Optimal design: $[x_{1,1}, x_{1,2}]$
$\tilde{p} = 1$	L.1	$2\left(1 - \left\{ \begin{array}{l} \frac{1}{\theta_1}\left[1 - e^{-\theta_1}\cosh(\theta_1 x_{1,1})\right] \\ \cdot \frac{1}{\theta_2}\left[1 - e^{-\theta_2}\cosh(\theta_2 x_{1,2})\right] \end{array} \right\} \right)$	[0,0]
$\nu = 3/2$	O.1	$2\left[1 - \frac{1}{2}\left(\frac{1}{\sqrt{3\theta_1}}\left\{ \begin{array}{l} 2\left[\begin{array}{l} 1 - e^{-\sqrt{3\theta_1}\,(1+x_{1,1})} \\ +1 - e^{-\sqrt{3\theta_1}\,(1-x_{1,1})} \end{array} \right] \\ -\sqrt{3\theta_1}\left[\begin{array}{l} (1+x_{1,1})e^{-\sqrt{3\theta_1}\,(1+x_{1,1})} \\ +(1-x_{1,1})e^{-\sqrt{3\theta_1}\,(1-x_{1,1})} \end{array} \right] \end{array} \right\} \cdot \frac{1}{\sqrt{3\theta_2}}\left\{ \begin{array}{l} 2\left[\begin{array}{l} 1 - e^{-\sqrt{3\theta_2}\,(1+x_{1,2})} \\ +1 - e^{-\sqrt{3\theta_2}\,(1-x_{1,2})} \end{array} \right] \\ -\sqrt{3\theta_2}\left[\begin{array}{l} (1+x_{1,2})e^{-\sqrt{3\theta_2}\,(1+x_{1,2})} \\ +(1-x_{1,2})e^{-\sqrt{3\theta_2}\,(1-x_{1,2})} \end{array} \right] \end{array} \right\} \right) \right]$	[0,0]
$\nu = 5/2$	P.1	$2\left[1 - \frac{1}{6}\left(\frac{1}{\sqrt{5\theta_1}}\left\{ \begin{array}{l} 8\left[\begin{array}{l} 1 - e^{-\sqrt{5\theta_1}\,(1+x_{1,1})} \\ +1 - e^{-\sqrt{5\theta_1}\,(1-x_{1,1})} \end{array} \right] \\ -5\sqrt{5\theta_1}\left[\begin{array}{l} (1+x_1)e^{-\sqrt{5\theta_1}\,(1+x_{1,1})} \\ +(1-x_1)e^{-\sqrt{5\theta_1}\,(1-x_{1,1})} \end{array} \right] \\ -5\theta_1\left[\begin{array}{l} (1+x_1)^2 e^{-\sqrt{5\theta_1}\,(1+x_{1,1})} \\ +(1-x_1)^2 e^{-\sqrt{5\theta_1}\,(1-x_{1,1})} \end{array} \right] \end{array} \right\} \cdot \frac{1}{\sqrt{5\theta_2}}\left\{ \begin{array}{l} 8\left[\begin{array}{l} 1 - e^{-\sqrt{5\theta_2}\,(1+x_{1,2})} \\ +1 - e^{-\sqrt{5\theta_2}\,(1-x_{1,2})} \end{array} \right] \\ -5\sqrt{5\theta_2}\left[\begin{array}{l} (1+x_1)e^{-\sqrt{5\theta_2}\,(1+x_{1,2})} \\ +(1-x_1)e^{-\sqrt{5\theta_2}\,(1-x_{1,2})} \end{array} \right] \\ -5\theta_2\left[\begin{array}{l} (1+x_1)^2 e^{-\sqrt{5\theta_2}\,(1+x_{1,2})} \\ +(1-x_1)^2 e^{-\sqrt{5\theta_2}\,(1-x_{1,2})} \end{array} \right] \end{array} \right\} \right) \right]$	[0,0]
$\tilde{p} = 2$	N.1	$2\left[1 - \sqrt{\frac{\pi}{16}}\left(\frac{1}{\sqrt{\theta_1}}\left\{ \begin{array}{l} erf\left[\sqrt{\theta_1}\,(1 + x_{1,1})\right] \\ +erf\left[\sqrt{\theta_1}\,(1 - x_{1,1})\right] \end{array} \right\} \cdot \frac{1}{\sqrt{\theta_2}}\left\{ \begin{array}{l} erf\left[\sqrt{\theta_2}\,(1 + x_{1,2})\right] \\ +erf\left[\sqrt{\theta_2}\,(1 - x_{1,2})\right] \end{array} \right\} \right) \right]$	[0,0]

Table 3.1. Normalized *IMSPE* formulas are given for the four correlation-parameter functions, along with the corresponding equation number of [3], as described in the text. Each optimal design is an origin point.

Figure 3.1, below, shows the value of the optimal design, $IMSPE_0$, as a function of θ_2, parameterized for fifteen values of θ_1.
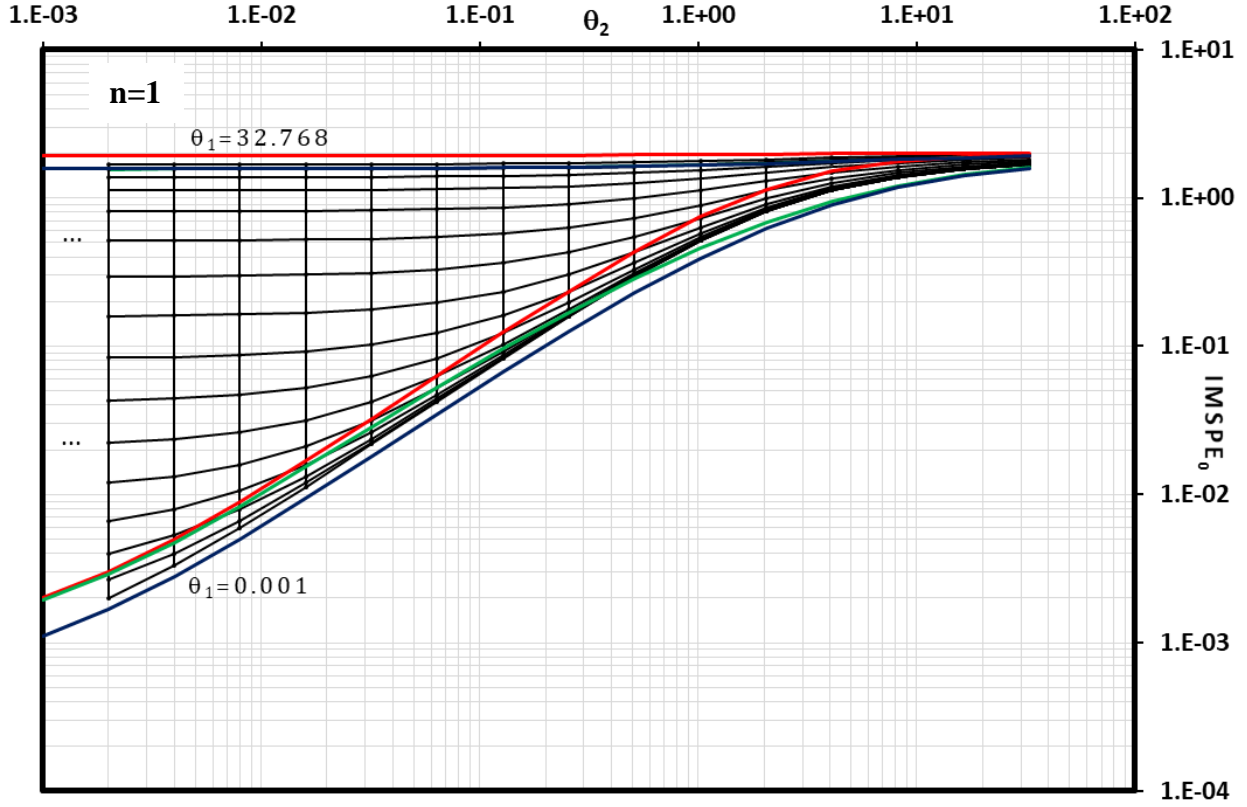

Fig. 3.1. Log-log $IMSPE_0$ vs. θ_2 plot for $0.001 \leq \theta_2 \leq 32.768$, parameterized by thirteen logarithmically spaced values of θ_1 in the same range, showing the general trend of increasing $IMSPE_0$ for increasing values of either θ_1 or θ_2, with the other θ_i, $i = 1,2$, fixed. The vertical lines are values of $IMSPE_0$ parameterized by logarithmically spaced values of θ_2. The form of the plot was chosen for consistency with the $n = 4$, Fig. 3 phase diagram of [2]. For $\theta_1 = 32.768$ and 0.001, red, green, blue, black lines are used to represent $IMSPE_0$ values for correlation-parameter functions $\tilde{p} = 1, \nu = 3/2, \nu = 5/2$, and $\tilde{p} = 2$, respectively. For $\theta_1 = 32.768$, the green and blue lines are indistinguishable.

3.2 $n = 2$

With two points, and over the same ranges of θ_1 and θ_2 used in Sec. 3.1's single-point case, each design is a specific case of one of the generic design types shown in Fig. 3.2.1, below. In what follows, we will call the five categories shown on the upper passage, traversing Fig. 2 from left to right, as the canonical categories.
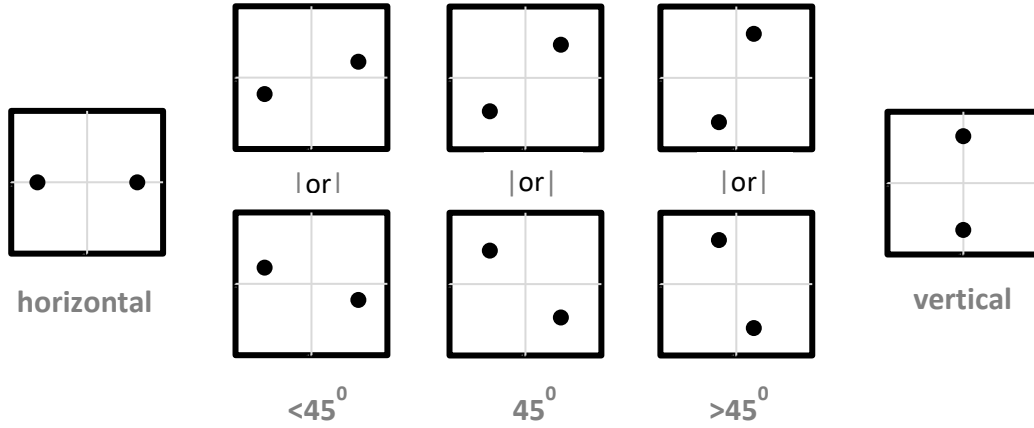
4

Fig. 3.2.1 Each two-point, two-factor, *IMSPE*-optimal design falls into one of the five, generic, inversion-symmetric categories shown in the above five columns. From left to right, we name these categories "horizontal," "$< 45°$" (by considering the absolute value of the smallest rotation angle between the abscissa and the line connecting the upper-diagram's points), "$45°$," "$> 45°$," and "vertical."

A key feature of the resulting phase diagram, Fig. 3.2.2 below, is the locus of points for which $\theta_1 = \theta_2$. This locus, which we have dubbed the "spine," is displayed in red in the Figure and consists exclusively of $45°$-diagonal-point designs. Attached to the spine are two proximal regions, the upper (resp., lower) of which is comprised of less- (resp., greater-) than-$45°$ diagonal points, displayed in yellow. The concatenation of the spine and these proximal regions constitute a bird's beak which narrows rapidly as one progresses from upper-right to lower-left in the Figure.

Fig. 3.2.3 demonstrates how the bird's beak narrows along the spine as $\theta_1 = \theta_2$ decreases. The abscissa is the same as in Fig. 3.2.2, while the ordinate is the half-range of values of θ_1 for which the optimal design has category $45°$. At $\theta_1 = \theta_2 = 0.001$, the slope is approximately -2.

Fig. 3.2.4 shows various characteristics of this bird's beak, including how the angle between the abscissa and the straight line between design points grows from zero to $90°$ and how the half-distance between design points increases and then decreases, both as functions of θ_2, using an abscissa, $(\theta_2 - \theta_1)/\theta_1$.
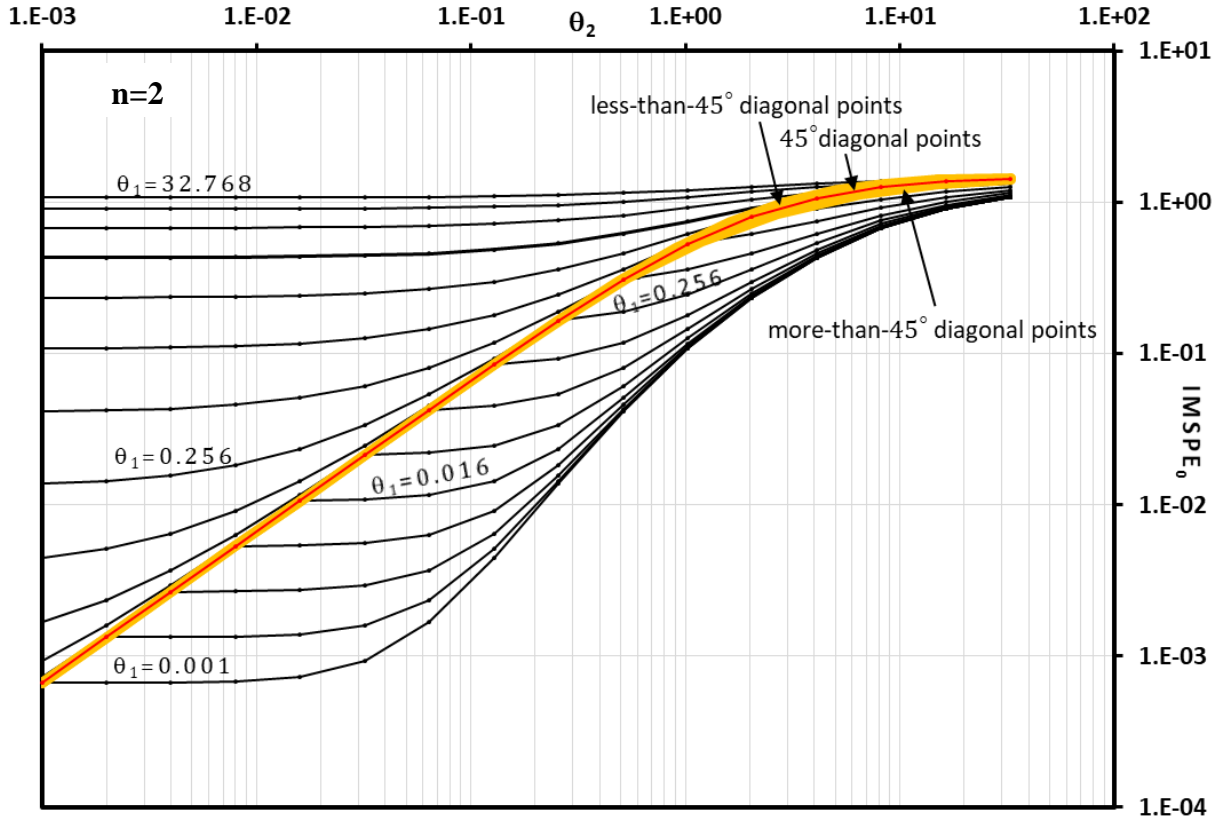
Fig. 3.2.2. This plot is similar to Fig. 3.1, but with two design points. The uncolored, upper-left (resp., lower-right) contiguous region has horizontal (resp., vertical) points. The upper (lower) of the two yellow regions have less-than- (resp., greater-than-) 45° diagonal points. The red line follows the $\theta_1 = \theta_2$ locus, along which all designs are in the category "45° diagonal points."
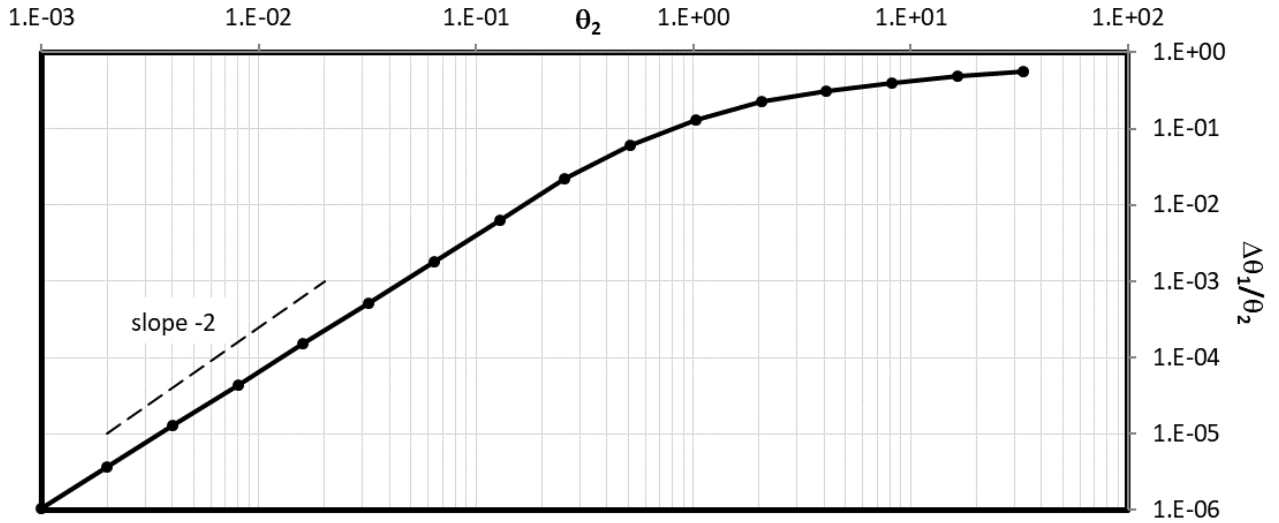

Fig. 3.2.3. The bird's beak narrows along the spine as $\theta_1 = \theta_2$ decreases. The abscissa is the same as in Fig. 3.2.2, while the ordinate is the half-range of values of θ_1 for which the optimal design has category 45°, divided by θ_2. At $\theta_1 = \theta_2 = 0.001$, the slope is approximately -2.
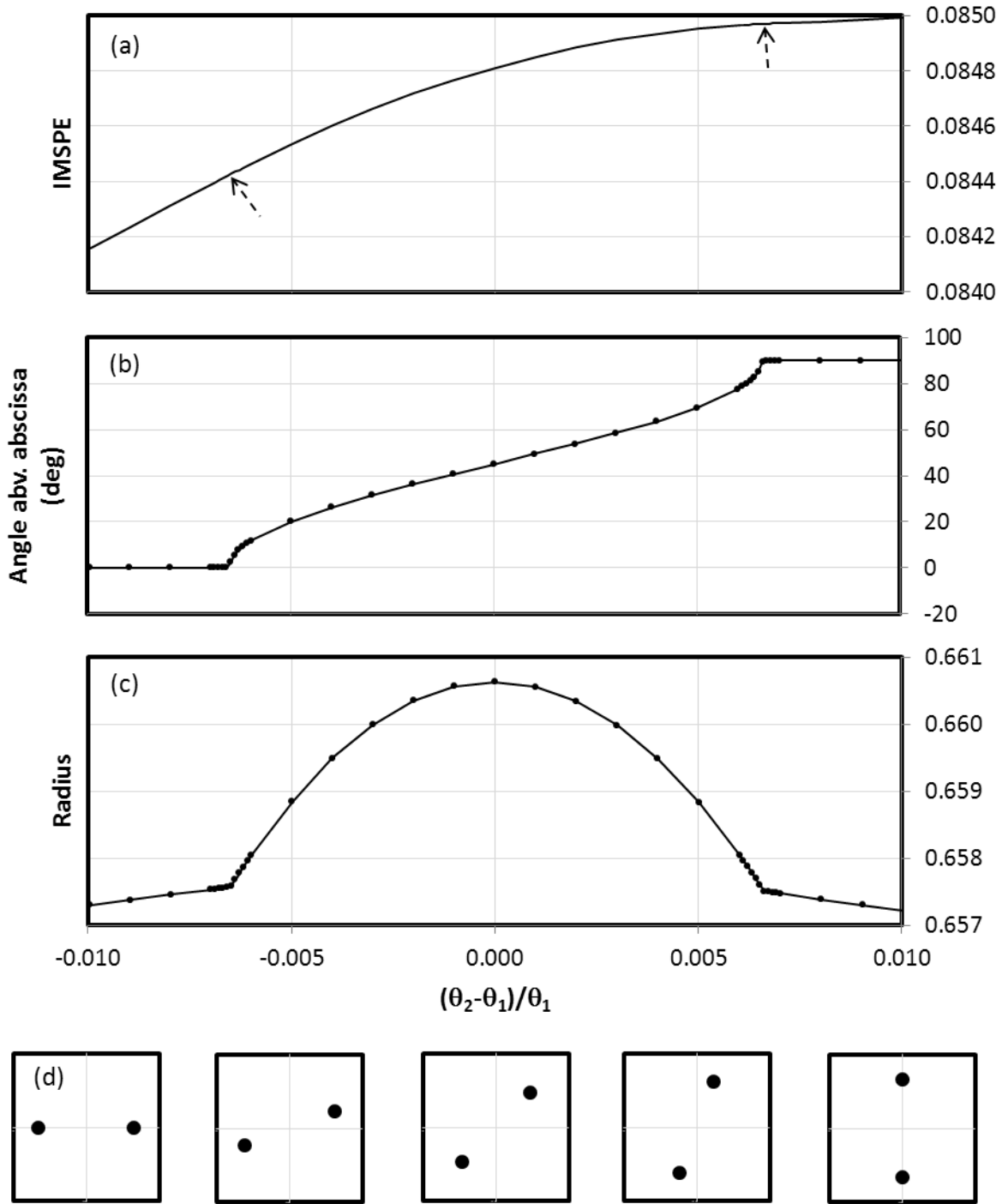
Fig. 3.2.4. With reference to Fig. 3.2.2's parameterized path $\theta_1 = 0.128$, this figure shows the following: (a) a three-segment, continuous plot of $IMSPE_0$ vs. $(\theta_2 - \theta_1)/\theta_1$, as the bird's-beak region is crossed, where the designs of the leftmost (resp., rightmost) segment are horizontal (resp., vertical) points. The central region contains designs in the other three categories; (b) the absolute value of the smallest angle from the abscissa to the straight line connecting the design points; (c) the half-distance (radius) between the design points; and, (d) cross-referenced from Fig. 3.2.1, the canonical categories of the design points as the bird's beak is crossed.

3.3 $n = 3$

With three points, each design is a specific case of one of the ten generic design types shown in Fig. 3.3.1, below.
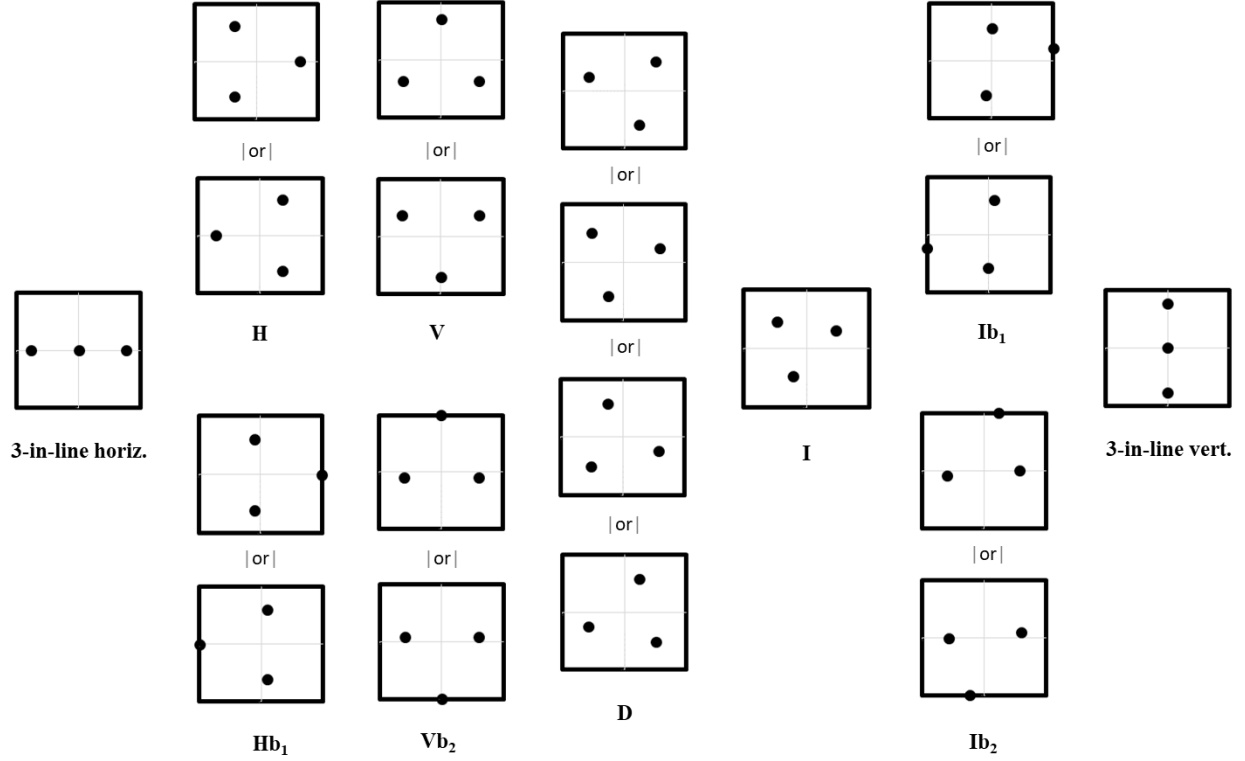

Fig. 3.3.1. Each three-point, two-factor, *IMSPE*-optimal design falls into one of the eleven, generic, inversion-symmetric categories shown in the above seven columns. By column, from left to right, these categories are labeled, in boldface, as follows: (Col. 1) "3-in-line horiz.," with obvious meaning; (Col. 2, upper) "H," denoting the design is symmetric under reflection about the abscissa (horizontal axis); (Col. 2, lower) "Hb$_1$," with "b$_1$" denoting the design has a point on the boundary of the first coordinate; (Col 3, upper) "V," with obvious meaning; (Col. 3, lower) "Vb$_2$;" (Col. 4, upper) "D," denoting the design is symmetric under reflection about the lower-left-to-upper-right diagonal of the square design domain; (Col. 4, lower) "D'," denoting the design is symmetric under reflection about the upper-left-to-lower-right diagonal; (Col. 5) "I," indicating the design has no mirror symmetry; (Col. 6, upper) "Ib$_1$;" (Col. 6, lower) "Ib$_2$;" and (Col. 7) "3-in-line vert."

The phase diagram for $\theta_2 \leq \theta_1$ is shown in Fig. 3.3.2, with the prominent $\theta_2 = \theta_1$ spine forming the lower-right boundary. The phases for $\theta_2 > \theta_1$ are not shown, but would follow under reversal of the indices of the coordinates, viz., $x_2 \leftrightarrow x_1$. For example, the near-spine H phase at $\theta_2 = \theta_1 - \varepsilon$, for small ε, becomes a V phase at $\theta_2 = \theta_1 + \varepsilon$.

8
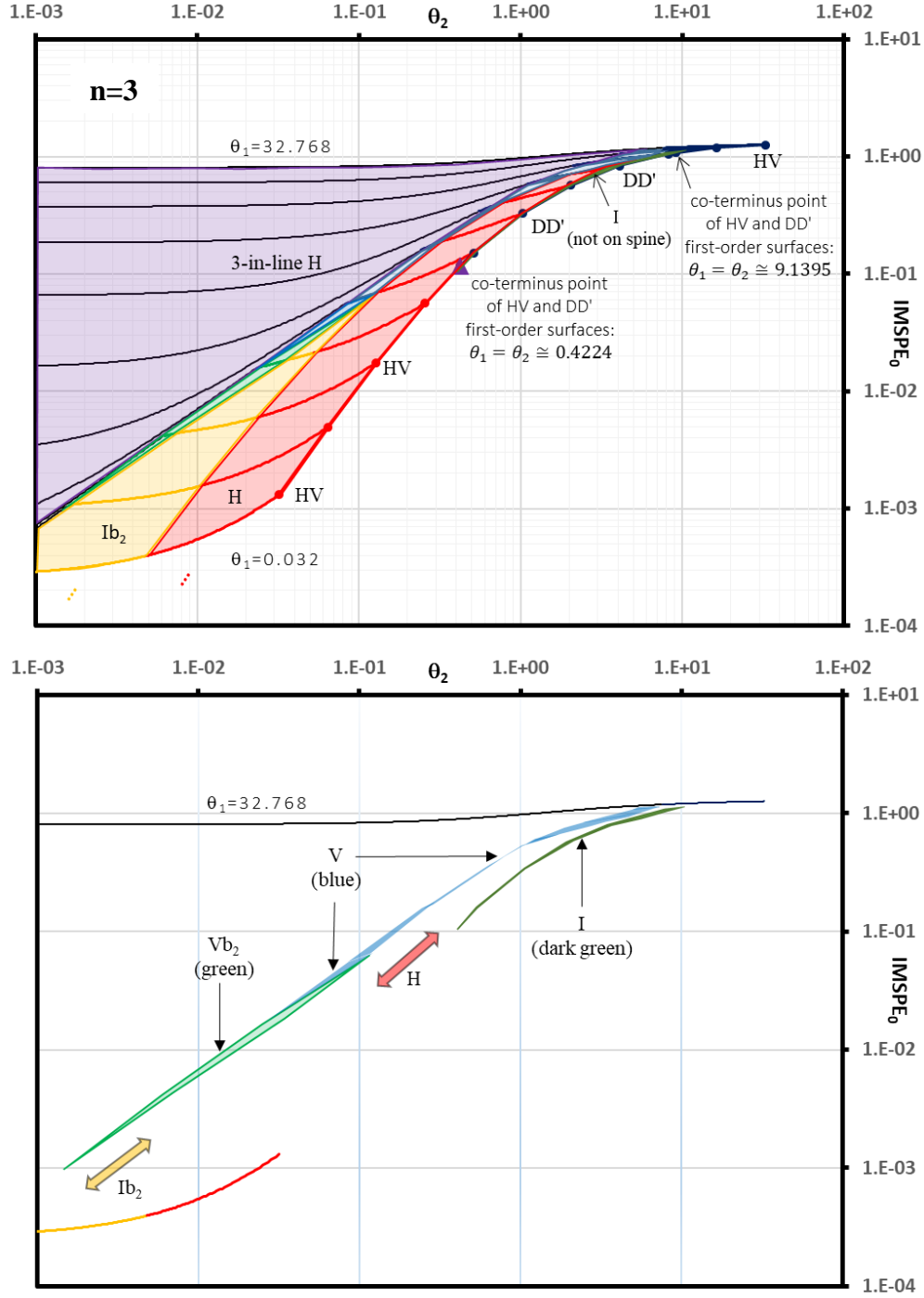
Fig. 3.3.2. (upper) This phase diagram for three design points is similar to Fig. 3.2.2, but only for the $\theta_2 \leq \theta_1$ domain. The design-point categories (and their colorings) are the following: 3-in-line (purple), Vb_2 (green), V (blue), Ib_2 (yellow), H (red), and I (dark green). For clarity, the symmetric extension to the right of the spine, is not shown. Loci, on the spine, of a multiple-point and a triple-point are shown. (lower) After removal of the large-area purple, yellow, and red colored regions; the small-area Vb_2, V, and I loci appear distinctly.

We conjecture that the lower-left or upper-right loci of the phases in Fig. 3.3.2. each has one of the following four fates: ending at a terminus, narrowing to a non-terminating bird's beak on a log-log plot of θ_2 vs. $IMSPE$, narrowing to a bird's beak on a lin-lin plot of θ_2 vs. $IMSPE$, or expanding in $IMSPE$ thickness. These conjectures are summarized in Table 3.3, below.

Phase	Lower/Upper end of θ_2 range	Character, from lower to upper, when appropriate
Vb$_2$	lower	log-log bird's beak
	upper	sorcerer's hat
V	lower	terminus, expanding in $IMSPE$ thickness
	upper	narrowing, filamentary, expanding in $IMSPE$ thickness
Ib$_2$	lower	bird's beak
	upper	sorcerer's hat
H	lower	bird's beak
	upper	sorcerer's hat
I	lower	terminus
	upper	expanding

Table 3.3. For each of the five phases in the above table's left column; then for the lower or upper end of the range of θ_2 of each of these phases, designated in the middle column; the right column reports the conjectured character(s) of the phases in Fig. 3.3.2. For example, the lower end of the Vb$_2$ phase is a non-terminating bird's-beak region on a log-log plot of θ_2 vs. $IMSPE$, while the upper end terminates in a sorcerer's hat. Another example: The V phase, for its upper-θ_2 values, narrows, becomes a thin filament, and then expands in $IMSPE$ thickness.

The phases on the lower-left and far-upper-right of the spine are two, first-order, co-dimension-one loci of coexisting H and V phases, which we name HV. Between these HV phases, but still along the spine, there are also first-order, co-dimension-one loci of coexisting D and D' phases, which we name DD'. These last loci have termini at $\theta_1 = \theta_2 = 0.4224$ and $\theta_1 = \theta_2 = 9.1395$, as shown in Fig. 3.3.2. These termini, as well as special off-spine points shall be discussed in a subsequent paper.

3.4 $n = 4$

The putatively complete phase diagram for four points was presented earlier [2].

3.5 $n = 11$

A coarse phase diagram for eleven points was presented earlier [4].

4. A four-factor optimal design

A four-factor, minimum-$IMSPE$-optimal design was presented earlier [4].

5. d-factor, $(d+2)$-point, d-uplet-point optimal designs on d-cubes

This section details a remarkable series of d-uplet-point, $n = (d+2)$-point designs over design domains with $1 \leq d \leq 6$ factors.

$(d, n; \theta_1) = (1, 3; \ 0.064)$

The *IMSPE*-optimal design in one factor and three design points is $x = \{-0.77076 \ldots, 0, 0.77076 \ldots\}$. Its dot diagram is given in Fig. 5.1, below.

$(d, n; \theta_1, \theta_2) = (2, 4; \ 0.064, 0.00008)$

With unit increases in d and n, the optimal design falls into the rhombus-with-twins phase of the Stormann phase diagram of [2]. Its dot diagram is given in Fig. 5.1, below.

$(d, n; \theta_1, \theta_2, \theta_3) = (3, 5; \ 0.064, 0.00008, 0.00008)$

With another unit increase in each of d and n, the *IMSPE*-optimal design found, after one-hundred random starts and application of the quadruple-precision qMINOS downhill-search optimizer [5] to each, was that given in Table 5.1, below. Its dot diagram is given in Fig. 5.1, below. Points numbered 3, 4, and 5 lie clustered on the $x_1 = 0$ plane, very close to the origin. Also given are the radial distances, $\sqrt{x_2^2 + x_3^2}$, from the origin, of these points; the angle of the radial vector of each of these points, defined as $tan(\varphi) \equiv x_3/x_2$, reported as $0 \leq \varphi < 360$ degrees; and the value of the design's *IMSPE*. We also defined a "root-mean-squared asphericality" as the RMS of these three distances divided by their average distance. This gave $RMS\_asphericality = 4.0\%$.

Pt. #	x_1	$10^7 x_2$	$10^7 x_3$	$10^7 \sqrt{x_2^2 + x_3^2}$	$\varphi \equiv tan^{-1}\left(\dfrac{x_3}{x_2}\right)$ *(degrees)*
1	$-0.77089788995\ldots$	$0.0\ldots$	$0.0\ldots$		
2	$0.77089788988\ldots$	$0.0\ldots$	$0.0\ldots$		
3	$0.0000000\ldots$	$40.0\ldots$	$176.0\ldots$	180	77
4	$0.0000000\ldots$	$-185.0\ldots$	$33.0\ldots$	188	170
5	$0.0000000\ldots$	$129.0\ldots$	$-121.0\ldots$	177	317
IMSPE	$0.00001202702016380660842324179005231 23922$				

Table 5.1. The design with lowest *IMSPE* found using the quadruple-precision optimizer is given in the above table, along with the design's *IMSPE*. Also given, for each of the three central design points, are the point's radial distance from the origin, $\sqrt{x_2^2 + x_3^2}$, and the angle of the point's vector above the x_2 axis, φ. It is clear that each central point lies within a central ball of radius 0.00002.

From the values in Table 5.1, the dihedral angles between the three vectors from the origin to each of the points numbered 3, 4, and 5 are $170° - 77° = 93°$, $317° - 170° = 147°$, and $(77° + 360°) - 317° = 120°$, respectively. If each of these dihedral angles were $120°$, then Points 3, 4, and 5 would be three vertices of an equilateral triangle. Thus, given the uncertainties of the values of x_2 and x_3, it is evident that further optimization of the design, carried out with

more precision, might well lead to a global minimum of $IMSPE$ with a triplet-point, equilateral-triangle-based design. Additional support for the possibility of such a triplet-point design is the order-unity value of the $RMS\_asphericality$.
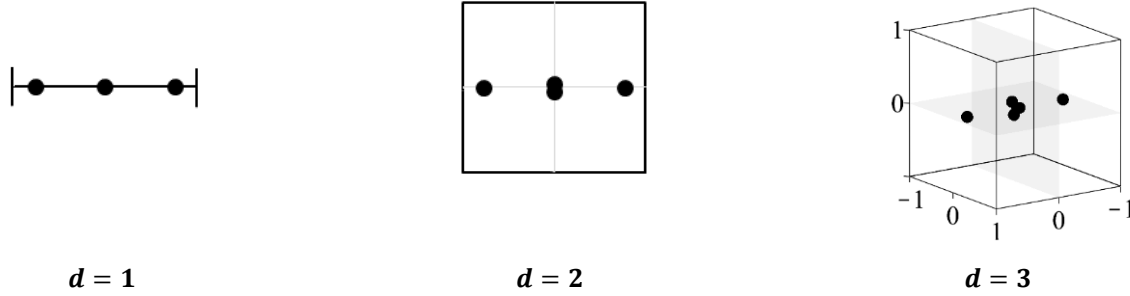

$d = 1$ $d = 2$ $d = 3$

Fig. 5.1. The first three in the series of $IMSPE$-optimal d-uplet-point designs are shown, above. In each case, $\theta_1 = 0.064$, and the other hyperparameters, if present, are $\theta_2 = \theta_3 = 0.00008$. Each design includes a d-uplet-point at the origin of its $[-1,1]^d$ design domain. Spacings of the central points are exaggerated for clarity. [left, $(d, n) = (1, 3)$] a central singleton point; [middle, $(d, n) = (2, 4)$] central twin points, with the vector normal to the common line of the twins along the axis with larger hyperparameter, which in this case is the abscissa; and [right, $(d, n) = (3, 5)$] central triplet points, with the vector normal to the common plane of the triplets along the axis with largest hyperparameter.

Refinement of the Table 5.1 design, using Maple [6] running with 100-digit precision, indeed revealed a triplet-point design with the triplet points coinciding with the vertices of an equilateral triangle (a.k.a. a regular 3-cell) lying in the $x_1 = 0$ plane, with φ taking one of the following twelve values: $(2m + 1)\pi/12$ radians, with $m = 0, 1, \ldots, 12$. After fixing the orientation at $\varphi = 5\pi/12$, an objective function of

$$IMSPE_0 = \binom{0.00001\ 20270\ 20163\ 80436\ 87372\ 41927\ 83048\ 72010\ 94549\ 86639}{\&05924\ 47074\ 26205\ 030171\ 4\ \ldots}$$

was found for the design in Table 5.2, below, via a convergence study of small radii of the vertices of the equilateral triangle from the origin, as well as single-point perturbations from this design. The ampersand denotes a continuation of the preceding line.

x_1		$10^{33}x_2$	$10^{33}x_3$
-0.77089789001453215877879203720419	45	0.0	0.0
0.77089789001453215877879203720419	45	0.0	0.0
0.00 …	00	cos(5π/12)	sin(5π/12)
0.00 …	00	cos(13π/12)	sin(13π/12)
0.00 …	00	cos(21π/12)	sin(21π/12)

Table 5.2. The IMSPE-optimal design found using 100-digit-precision refinement of the design of Table 5.1 is given.

The convergence study of the $IMSPE$ vs. radial distances from the origin of the triplet points demonstrated quadratic convergence, as shown in Fig. 5.2, below. In addition, the $IMSPE$ of the equilateral triplet in the (x_2, x_3) plane is modulated as it rotates about the origin, as shown in

12

Fig. 5.3, below, which uses a polar-coordinate version of the objective function, $IMSPE(r, \varphi)$. We surmise this modulation is a boundary effect that would not be present if the coincident design and prediction domains were a unit-radius ball. We also surmise that the triplet-point design would survive a change in the coincident design and prediction domains to such a unit-radius ball. Support for this surmise is given by the fact that the Stormann twin-point design survived a change in its boundary from the interior of a square to a disk [7].
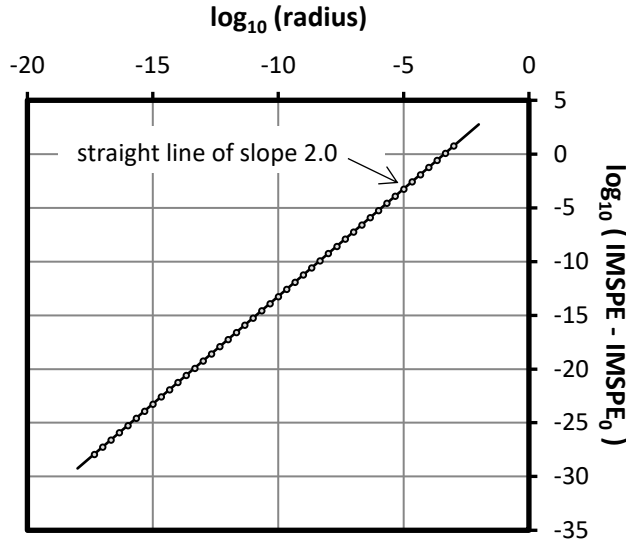

Fig. 5.2. This log-log plot shows the parabolic convergence of the $IMSPE$ to $IMSPE_0$, vs. radius, for radii in the range 10^{-3} to 10^{-18}.
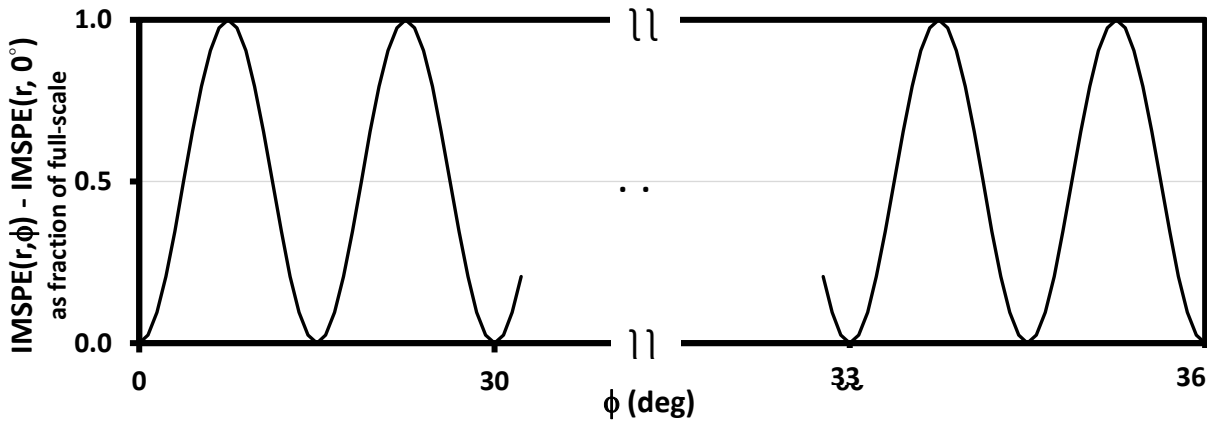

Fig. 5.3. The $IMSPE$ expressed in polar coordinates, i.e., $IMSPE(r, \varphi)$, is periodically modulated as the triplet rotates rigidly about the origin by angle φ in the (x_2, x_3) plane, with a repeat angle of $15°$. The relative modulation is independent of r. The amplitude of the modulation vanishes in the limit $r \to 0$.

More generally, the putatively optimal designs form a set whose members are one of the designs given in Table 5.3, below, for $m = 0, 1, 2$ or 3, or any of the 5! trivial permutations of point numbers, i.e., row permutations. Designs formed by the interchange $x_2 \leftrightarrow x_3$, i.e., column exchange, are already included in the ultimate-sentence's count, as can be seen by the identity $cos(\alpha) = sin(\alpha + 6\pi/12)$.

13

x_1	$10^{33}x_2$	$10^{33}x_3$
`-0.77089789001453215877879203720 41945`	0.0	0.0
`0.77089789001453215877879203720 41945`	0.0	0.0
`0.00          …          00`	`cos[(2m+ 5)π/12]`	`sin[(2m+ 5)π/12]`
`0.00          …          00`	`cos[(2m+13)π/12]`	`sin[(2m+13)π/12]`
`0.00          …          00`	`cos[(2m+21)π/12]`	`sin[(2m+21)π/12]`

Table 5.3. The $IMSPE(r, \varphi)$ of the design in the Table is invariant under changes in m, for $m = 0, 1, 2, 3$. For example, the argument of the cosine in the table's third row and second column can be $5\pi/12, 7\pi/12, 9\pi/12$, or $11\pi/12$. After trivial allowance for permutation of rows, the argument of the cosine in that location of the table can be any one of the set $\{\pi/12, 2\pi/12, 3\pi/12, \cdots, 23\pi/12\}$ of angles spaced by $\pi/12$ radians or $15°$.

$(d, n) = (4, 6), (5, 7)$, and $(6, 8)$, with $\theta_1 = 0.064$ and $\theta_2 = \theta_3 = \cdots \theta_d = 0.00008$

For the three cases in the sub-heading, the best designs found using the qMINOS quadruple-precision optimizer [5], along with the corresponding values of $RMS\_asphericality$, are given in Table 5.4, below. For the first (resp., second; third) case, the best design was the 77'th of 100, (resp., 85'th of 100; 3'rd of 10) random starts.

d	n	Cluster type	Pt. #'s	X1	X2	X3	X4	X5	X6	10^5* IMSPE	RMS asphericality (%)
1	3	single-ton	1,2	±0.77076…						0.763…	0
			3	0							
2	4	twin	1,2	±0.77082…	0					0.982…	0
			3,4	0	±0						
3	5	triplet	1,2	±0.77089…	0	0				1.202…	0
			3 to 5	0	Table 5.1						
4	6	quad-ruplet	1,2	±0.77096…	0	0	0			1.422…	49
			3 to 6	0	$r < 0.00004$						
5	7	quin-tuplet	1,2	±0.77103…	0	0	0	0		1.643…	69
			3 to 7	0	$r < 0.0002$						
6	8	sex-tuplet	1,2	±0.77110…	0	0	0	0	0	1.864…	59
			3 to 8	0	$r < 0.001$						

Table 5.4. The $IMSPE$-optimal designs, values of $IMSPE$, and $RMS\_asphericality$ are tabulated, above, for the series of designs discussed in the main text, with $n = d + 2$, $\theta_1 = 0.064$, and $\theta_2 = \theta_3 = \cdots = \theta_d = 0.00008$. The loci of the triplet of central points is given, as indicated, in the earlier Table 5.1. The loci of the quadruplet of central points is vague, due to insufficient numerical precision, although we report, for the lowest-$IMSPE$ design found, that the maximum radial distance r of any central point from the origin was less than 0.00004, and the $RMS\_asphericality$ was 49%. The corresponding values for quintuplet-point and sextuplet-point designs are also given. Cells with green backgrounds are expected to change to much lower values, possibly consistent with zero, upon future analysis with higher-precision arithmetic.

We were led to the conjecture that, upon further optimization, the central points in each of these three cases, would be vertices of a uniform tetrahedron (a.k.a. a regular 4-cell), a regular 5-cell, and a regular 6-cell, respectively. Further, we conjectured that this trend generalized to the existence of optimal-design phases with central points on the vertices of a d-cell for the general case $n = d + 2$, within, of course, suitable ranges of the corresponding hyperparameters.

6   Multiple-cluster optimal designs

We report the discovery of a putatively $IMSPE$-optimal design with two pairs of twin points, what we dub a "duet twin." This design's parameters, hyperparameters, and $IMSPE$ were $(d, n; \theta_1, \theta_2; IMSPE) = (2, 17; 0.128, 0.006; 2.9108\text{x}10^{-10})$. The design search used 1,000 random starts of the quadruple-precision program qMINOS [5], followed by refinement of the best design, using Maple [6] running with 40-digit precision. The resulting dot diagram is given in Fig. 6.1, below. A very long qMinos run with 10,000 random starts was made in order to generate the detailed histogram shown in Fig. 6.2. 62% of the designs found in this run had $IMSPE$ values within 0.4% of the putative global minimum.
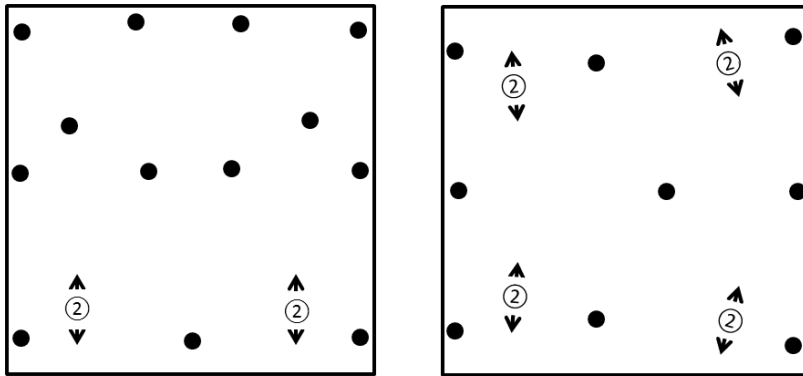

Fig. 6.1. (left) The above $(d, n; \theta_1, \theta_2; IMSPE) = (2, 17; 0.128, 0.006; 2.9108\text{x}10^{-10})$ design is the first putatively $IMSPE$-optimal design with two pairs of twin points. The circled "2"s with arrowheads denote respectively the twins' centers and the bi-directions connecting proximal points. The arrowhead on the RHS (resp., LHS) is tilted slightly counter-clockwise (resp., clockwise) of vertical. The design is symmetric about reflection about the ordinate. Another duet-twin design with identical objective function can be generated by reflection about the abscissa. (right) In the course of finding the putatively optimal design on the LHS, we also discovered the locally optimal, quartet-twin design on the RHS, via manual forcing of symmetry followed by Maple [6] refinement using 60-digit precision. This design is symmetric about reflection about the abscissa, as well as symmetric under inversion. A second quartet-twin design with identical objective function can be generated by reflection about the ordinate.
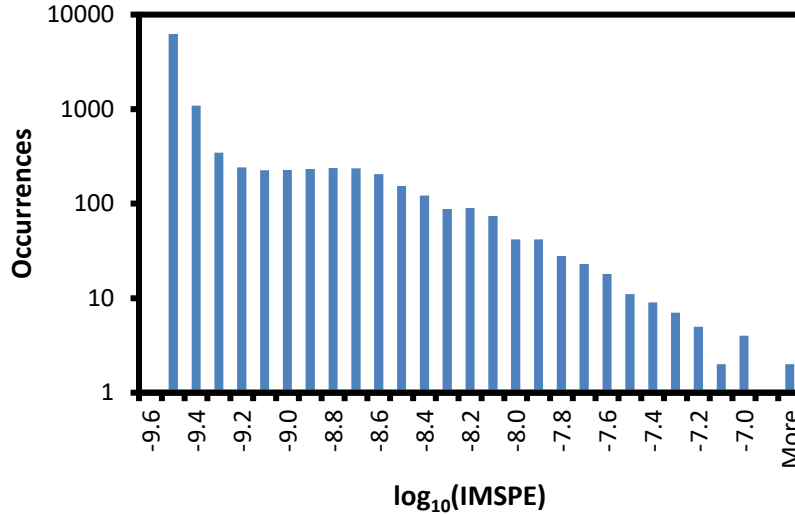
Fig. 6.2. Downhill searches of 10,000 random starts of the $(d, n; \theta_1, \theta_2) = (2, 17; 0.128, 0.006)$ problem yielded this histogram of the occurrences of the *IMSPE*.

7. Summary

We have demonstrated three, two-factor, *IMSPE*-optimal phase diagrams, as well as a variety of isolated *IMSPE*-optimal designs, notably including a triplet-point design with the triplet's inter-point separations less than 10^{-33}, as well as a duet–twin-point design.

8. Research reproducibility

We support the recommendations of ICERM's Workshop on Reproducibility in Computational and Experimental Mathematics Workshop [8]. All data and figure-generation files used in this research are available to responsible parties, upon request to selden_crary (at) yahoo (dot) com.

References

1. J. Sacks, S.B. Schiller, and W.J. Welch, "Designs for Computer Experiments," *Technometrics* **31** (1), pp. 41-47 (1989).
2. Selden Crary and Jan Stormann, "Four-Point, 2D, Free-Ranging, IMSPE-Optimal, Twin-Point Designs," arXiv:1510.01685 [stat.ME] 6 Oct 2015.
3. Selden Crary, "The Nu Class of Low-Degree-Truncated, Rational, Generalized Functions. I. IMSPE in Design of Computer Experiments: Integrals and Very-Low-N, Single-Factor, Free-Ranging Designs," arXiv:1604.05278 [stat.ME] 18 Apr 2016.
4. Selden B. Crary, "New Research Directions in Computer Experiments: ε-Clustered Designs," Spring Research Conference (SRC 2012), Cambridge, MA, June 13-15, 2012, presentation published in *JSM Proceedings*, Statistical Computing Section, Alexandria, VA, USA: ASA, pp. 5692-5706 (2012). URL: http://www.asasrms.org/Proceedings/y2012/Files/400245_500701.pdf.*
5. Bruce A. Murtagh and Michael A. Saunders, "A Projected Lagrangian Algorithm and its Implementation for Sparse Nonlinear Constraints," *Mathematical Programming* **16**, pp. 84-117 (1982).
6. Maple 2015, Maple 2016, …, or Maple 2018 [Computer Software], Maplesoft Software, Waterloo, ON Canada.

7. Nikoloz Chkonia and Selden Crary, "The Nu Class of Low-Degree-Truncated, Rational, Generalized Functions. Ic. IMSPE-optimal designs with circular-disk prediction domains," arXiv:1709.09599 [stat.ME] 27 Sep 2017.

8. V. Stodden, D. H. Bailey, J. Borwein, R. J. LeVeque, and W. Stein, eds., "Setting the Default to Reproducible: Reproducibility in Computational and Experimental Mathematics," webpage of the Reproducibility in Computational and Experimental Mathematics Workshop, held Dec. 9-14, 2012 at the Institute for Computational and Experimental Research in Mathematics, Providence, RI, and available at https://www.carma.newcastle.edu.au/jon/icerm12.pdf.

*Revisions are available from the first author at email address: selden_crary (at) yahoo (dot) com.